ACS APPLIED MATERIALS & INTERFACES

Research Article

www.acsami.org

Fully-Sprayed and Flexible Organic Photodiodes with Transparent Carbon Nanotube Electrodes

Aniello Falco,*[,†] Lucio Cinà,[‡] Giuseppe Scarpa,[†] Paolo Lugli,[†] and Alaa Abdellah[†]

[†]Institute for Nanoelectronics, Technische Universität München, Arcisstrasse 21, D-80333, München, Germany

[‡]CHOSE (Centre for Hybrid and Organic Solar Energy), Department of Electronic Engineering, University of Rome-Tor Vergata, via del Politecnico 1, 00133 Rome, Italy

Supporting Information

ABSTRACT: In this study, we demonstrate the feasibility of TCO-free, fully sprayed organic photodiodes on flexible polyethylene terephthalate (PET) substrates. Transparent conducting films of single-wall carbon nanotubes are spray deposited from aqueous solutions. Low roughness is achieved, and films with sheet resistance values of 160 Ω/sq at 84% in transmittance are fabricated. Process issues related to the wetting of CNTs are then examined and solved, enabling successive spray depositions of a poly(3,4-ethylenedioxythiophene):poly(styrenesulfonate) (PEDOT:PSS) layer and a blend of regioregular poly(3-hexylthiophene-2,5-diyl) and [6,6]-phenyl C61 butyric acid methyl ester (PCBM). The active layer is then optimized, achieving a process yield above 90% and dark currents as low as 10^{-4} mA/cm^2. An external quantum efficiency of 65% and high reproducibility in the performance of the devices are obtained. Finally, the impact of the characteristics of the transparent electrode (transmittance and sheet resistance) on the performances of the device are investigated and validated through a theoretical model and experimental data.

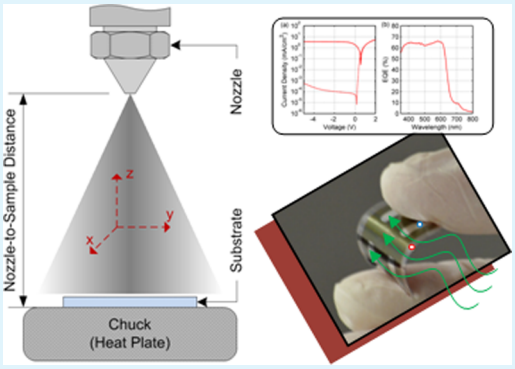

KEYWORDS: *flexible, organic photodiode, spray deposition, carbon nanotubes, solution processable, bulk heterojunction*

INTRODUCTION

Organic photosensitive devices have raised increasing interest among a multidisciplinary community of researchers. Designs based on solution-processable bulk heterojunction (BHJ) thin films were successfully applied to solar cells, photodiodes, and phototransistors.[1−3] There a photoactive conjugated polymer is intimately blended with an electron acceptor, usually a fullerene, to form an interpenetrating network of both materials. Organic photodiodes (OPD) offer some major advantages as compared to their inorganic counterparts. Adjustable spectral sensitivity, large active areas, mechanical flexibility, and facile monolithic integration are some particularly attractive features. In general, low-cost additive manufacturing by means of simple coating and printing techniques is a great advantage of this technology.

Meanwhile, random networks of carbon nanotubes (CNT) have evolved as an exciting material for the organic and printed electronics industry. The remarkable and concurrently diverse properties of such networks have rendered them suitable for a wide range of applications in science and engineering.[4−6] One interesting application is to be found in the field of solution-processable transparent conductors. Thin films of CNTs can serve as alternative transparent electrodes in organic optoelectronic devices, achieving reasonable trade offs with respect to sheet resistance and transmittance.[7−9] As opposed to the commonly used indium tin oxide (ITO), CNT-based electrodes further exhibit superior mechanical stability when deposited onto flexible substrates[10,11]

In order to fully exploit the potential of large-area printed electronics based on organic semiconductors and nanomaterials, it is necessary to achieve high-throughput, low-cost production onto a wide range of substrate materials. Spray deposition provides a technology platform capable of fulfilling these requirements. It has been recently utilized for fabrication of conjugated polymer and carbon nanotube thin films, which were evaluated within the context of different device applications.[9,12−19] However, extensive research and development is still required to achieve reliable and reproducible spray deposition of multilayer stacks of different functional materials. This allows for simpler process integration, paving the way for fully sprayed photosensitive devices.

Although the feasibility of CNT-based transparent electrodes has been previously investigated for organic solar cells (OSC)[9,20] and light-emitting diodes (OLED),[8] their use in OPDs was largely neglected. Further, no complete study of a fully sprayed flexible optoelectronic device incorporating CNT-based electrodes has been reported to date. In a first attempt to realize fully sprayed OPDs, Tedde et al. demonstrated devices

Received: April 14, 2014
Accepted: June 10, 2014
Published: June 10, 2014

exhibiting high sensitivities, long shelf life, and highly reproducible low dark currents at high reverse bias.[12] Binda et al. realized an integrated fiber/receiver system, exploiting a spray-coating technique for deposition of solution-processable OPDs onto highly nonplanar and unconventional substrates.[21] However, in both studies only the hole injection and active layers were solution processed. A similar approach was pursued by Na et al. to obtain spray-coated solar cells[22] and by Girotto et al.[13] Recently, La Notte et al. reported fully sprayed organic solar cells with transparent-conducting oxide (TCO) electrodes where high-temperature spray pyrolysis was used to deposit TiO_2 on glass substrates.[23]

On the other hand, organic solar cells with spray-deposited CNT electrodes were fabricated either by air-assisted[14] or ultrasonic spray technology[9] yielding very promising results. Nevertheless, hole injection and active layers were always deposited using more conventional and less scalable deposition methods such as spin coating.

Hence, despite the systematic work conducted on the fabrication of the organic layers and semitransparent electrodes, no effort was so far done to spray such multilayer stacks onto nanotube/nanowire network electrodes at low temperatures.

Here we demonstrate TCO-free fully sprayed organic photodiodes on flexible substrates incorporating CNT-based electrodes. Understanding the critical aspects of multilayer spray deposition was of foremost importance in order to obtain state-of-the-art photodiodes with high yields. We start by presenting the CNT electrode deposition and motivating the choice of the dispersant. The CNT/PEDOT:PSS critical interface is analyzed, and two methods to enhance the wettability of the CNT layer are compared. The realized photodiodes are evaluated in terms of $J-V$ characteristics and external quantum efficiency. Then the effect of the thickness of the BHJ on the devices overall performances is verified, and its influence on the yield is investigated through spatially resolved EQE measurements. Finally, the trade off between sheet resistance and transmittance of the CNT electrode is examined through the aid of a simple theoretical model and validated with experimental data.

EXPERIMENTAL METHODS

CNT deposition was performed through an automated spray system with an industrial air atomizing spray valve (Nordson EFD, USA) mounted on an overhead motion platform (Precision Valve & Automation, USA). The most important parameters to be adjusted for obtaining desired spray characteristics are material flow rate, atomizing gas (N_2) pressure, nozzle-to-sample distance, substrate temperature, and motion speed. The diameter of the orifice is one of the most significant dimensions for atomization in air-assisted nozzles. Here a nozzle with a 0.3 mm orifice diameter was chosen. The polymer depositions setup (used for PEDOT:PSS and for P3HT:PCBM blends) was composed of two identical commercially available spray guns (Krautzberger GmbH, Germany) connected to a pneumatic controller. The atomizing gas is pressurized N_2, and the pressure was always kept below 1 bar in order to obtain smoother depositions. The nozzle-to-sample distance was kept constant to 15 cm; the material flow and substrate temperature were consequently regulated to obtain the desired thicknesses with spraying times ranging between 10 and 25 s.

For the dispersion of CNTs in aqueous solution, SDS or CMC are solved in distilled water in a weight ratio of 0.5% wt. The CMC solution is stirred overnight for at least 12 h at room temperature, while the SDS solution only needs 1 h stirring. When the solutions are uniform, 0.05 wt % of SWNTs (Hanwha Nanotech) is added and the CMC and SDS solutions are sonicated for 20 and 30 min, respectively, by means of a horn sonicator (Branson Sonifier S-450D) to obtain a uniform dispersion of the carbon nanotubes. Solutions are finally centrifuged at 15 000 rpm for 90 min.

The bulk heterojunction blend is obtained dissolving solid-phase regioregular poly(3-hexylthiophene-2,5-diyl) (Rieke Metals Inc.) and [6,6]-phenyl C61 butyric acid methyl ester (PCBM) (Solenne B.V.) in o-DCB (Sigma-Aldrich) with a 1 wt %:1 wt % ratio and stirred overnight (>12 h) at 60 °C. The PEDOT:PSS (CLEVIOS P VP CH 8000) solutions were sprayed in a dilution of either 1:3 with DI water or 1:3 in isopropyl alcohol (Sigma-Aldrich).

The thickness and uniformity of the CNT layer and PEDOT:PSS were evaluated via atomic force microscopy images and using a Dektak II mechanical profilometer. Bulk heterojunction thickness was evaluated with means of the Dektak II profilometer only. The sheet resistance was measured using a custom-made four-points probe and a Keithley 4200 semiconductor parameter analyzer. The transmittance of the CNT film and EQE of the devices were measured using a 300 W xenon arc lamp choppered at 210 Hz, passing through an Oriel Cornerstone 260 1/4 m monochromator and a calibrated photodiode with a transconductance amplifier connected to an Oriel Merlin digital lock-in amplifier. Finally, the IV characterization of the OPDs were performed by means of a Keithley 2602 sourcemeter, dark current measurements were performed inside a dark chamber, and photocurrent measurements were performed under illumination with a tungsten halogen source at 100 mW/cm^2. Spatially resolved EQE were measured by means of an inverted microscope (Leica DMI 5000) coupled with a monochromator (m Cornerstone 130) in turn preceded by a xenon lamp (200 W Apex mod. 66450). The wavelength was fixed to 550 nm (±2 nm). A long working distance objective with 100× of magnification yields a 30 × 30 μm of spot area. The device area was scanned with step of 30 μm by a $x-y$ motorized stage. A calibrated silicon photodiode is mounted with a beam splitter at the optical entrance of the microscope in order to monitor the incident optical power. The short circuit photocurrents of both device and calibrated photodiode are discriminated in a phase-sensitive detection system composed by an optical chopper (210 Hz of modulation) and two digital lock-in amplifiers (EG&G 7265)

RESULTS AND DISCUSSION

In order to obtain a fully sprayed device, deposition of the anode material had first to be optimized. A random network of carbon nanotubes, which can be deposited from solution, is chosen as transparent electrode. As well known,[6,24] single CNTs are strongly attracted by van der Waals forces, needing therefore a dispersant to avoid creation of clusters (bundles) that degrade the film quality in terms of transmittance and roughness. After spraying, the dispersant is chemically removed and a network of randomly oriented CNTs is formed. If the density of CNTs is high enough, the percolation threshold is reached[6,9] and electric paths are established throughout the whole film.

Two of the most commonly used dispersants are sodium dodecyl sulfate (SDS) and carboxymethyl cellulose (CMC). The former is a weaker dispersant, leading to formation of large CNT bundles if compared to the latter. The most important consequence is that the roughness of the CNT film is considerably higher in the case of SDS,[25] suggesting CMC as a more suitable dispersant for fabrication of CNT electrodes for multilayer devices. However, in order to remove the CMC from the as-prepared film, several hours of acid treatment are needed, while SDS can be simply removed via immersion in water for less than 1 h. Once the film has been deposited and the dispersant removed, it can be electro-optically characterized measuring its sheet resistance and transmittance spectrum.

The relationship between transmittance and sheet resistance in a CNT film as well as in many other transparent-conductive films can been analyzed through Tinkham's formula[26]

$$T = \left[1 + \frac{\zeta_0}{2R_{sh}}\frac{\sigma_{op}}{\sigma_{dc}}\right]^{-2} = \left[1 + \frac{\zeta_0}{2R_{sh}}\frac{1}{\gamma}\right]^{-2} \quad (1)$$

where T is the transmittance, R_{sh} the sheet resistance, σ_{dc} is the dc electrical conductivity (assumed to be independent of thickness), and σ_{OP} is the optical conductivity of the film. $\xi_0 = 120\pi$ is the impedance of free space. The ratio between σ_{dc} and σ_{OP} is referred as γ, and it is used as a figure of merit for the quality of the film: the higher γ, the lower the sheet resistance at a given transmittance. Figure 1 shows the experimental values

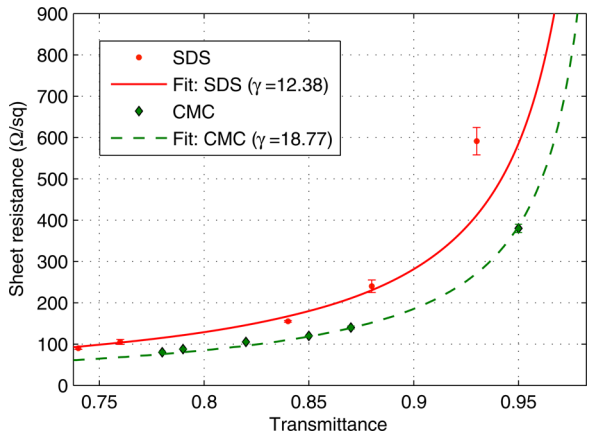

Figure 1. Experimental data (markers) and Tinkham formula fit (lines) for CNT films from SDS (squares) and in CMC (diamonds) dispersed solutions with no further doping after dispersant removal.

of transmittance at 550 nm and sheet resistance for films of different thickness. These values are then fitted to the Tinkham formula, and values for the figure of merit γ are obtained.

These fits result in an estimated γ of 18.77 and 12.38 for CMC and SDS, respectively. It must be noticed that the nitric acid treatment used to remove the CMC also introduces an unintentional doping to the CNTs that reduces the sheet resistance of the film.[6,27] A reasonable working point for fabrication of photodiodes can be found for transparent electrodes obtained with both dispersants (e.g., 120 Ω/sq with 85% in transmittance and 160 Ω/sq with 84% in transmittance for CMC and SDS, respectively). Nevertheless, since the differences between the quality of the thin films obtained with the two dispersants is not particularly wide, the choice of one over the other can be motivated with different arguments. Particularly, the choice of avoiding acid treatments, and hence opt for SDS, can be strongly convenient since it keeps the process as simple as possible and enables cheap and "green" manufacturing. Moving in the same direction, although standard[28] or interlayer lithography[29] of CNTs has been widely reported and used, the patterning of the CNT film was performed via shadow masking, i.e., spraying through a stencil without any further treatment.

Once the anode contact has been deposited, the PEDOT:PSS interlayer must be fabricated on top of it. In order to obtain a uniform deposition of the polymers and enable a fine tuning of the thickness, it is necessary to choose the correct spray deposition regime. It is common practice[18] to distinguish between three different working regions: dry, wet, and intermediate. In the first case, the solvent evaporates before arriving on the substrates and no proper layer is formed. On the other hand, the wet regime corresponds to formation of a liquid polymer layer, hence inhomogeneous and with a poor control on the thickness. In the intermediate regime, finally, separate droplets impact with the sample and partially merge together forming more uniform and smoother layers. Nevertheless, spray deposition in the intermediate regime is not enough to guarantee full coverage and uniform deposition. The droplets forming the layer must spread, and their height must be kept low, which means that the lower the contact angle and the surface tension of a droplet of the sprayed material on the given substrate, the better is the film formation.

The straightforward fabrication of photodiodes using PEDOT:PSS in aqueous solution on a CNT film without any modification resulted in a yield, here defined as the ratio between the number of functioning devices over the number of fabricated devices, lower than 50% (See Table 1). The working

Table 1. Process Yield for the Different Used Deposition Approaches, Defined as the Ratio of the Number of Properly Functioning Devices to the Total Number of Fabricated Device with a Given Treatment Combination

CNT	PEDOT:PSS	blend thickness	fabrication yield
untreated	1:3 in H_2O	800 nm	~38% (6/16)
O_2 plasma	1:3 in H_2O	800 nm	~56% (9/16)
untreated	1:3 in IPA	800 nm	~94% (15/16)
		650 nm	~75% (12/16)
		500 nm	~50% (8/16)
		350 nm	~19% (3/16)

devices presented, as shown in Figure 2, average peak EQE comprised between 45% and 55%, dark currents densities of 10^{-3} mA/cm^2 at −5 V, and rectification ratios of 3 orders of magnitude.

It must be here noticed that the high hydrophobicity of CNTs[14,30] is a known issue. In our case, the PEDOT:PSS in aqueous solution presented a contact angle as high as 50° (Figure 3) on the bare CNT film, a characteristic that usually prevents obtainment of reliable processes for solution-based techniques.

Several solutions were proposed in the literature for reduction of the contact angle and improvement of the wetting. Typically, they are focused on either enhancing the hydrophilicity of the CNT layer or reducing the surface tension of the formed droplets by tuning the ink formulation. To the first class of methods belong prewetting of the sample with water-soluble alcohols[14] or plasma treatment of the surface,[30] while to the second class of solutions belong wetting agents or use of a so-called "two-solvent system".[13] The approaches that demonstrated to be more effective for this work were a mild oxygen plasma treatment and dilution of the PEDOT:PSS aqueous solution in 2-isopropyl alcohol (IPA), which acted as a cosolvent in the water−IPA two-solvent system.

As reported in the literature, oxygen plasma treatment is known to ameliorate the wettability of many materials used as thin films in nanoelectronics, such as P3HT:PCBM,[31] ITO,[32] and of CNTs.[30] The natural first choice was hence trying a mild oxygen plasma treatment which is strong enough to activate the CNT surface but mild enough to prevent noticeable damage to the film. The weaker plasma treatment that still guaranteed an

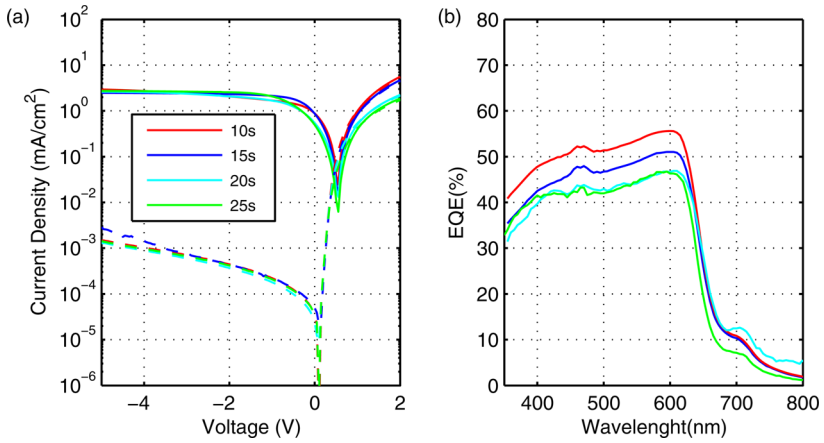

Figure 2. (a) Dark (dashed lines) and illuminated (solid lines) *JV* characteristics of OPDs obtained spray-coating PEDOT:PSS in aqueous solution and P3HT:PCBM blend on structured CNTs, increasing spraying time of the PEDOT:PSS layer. (b) EQE of the same samples.

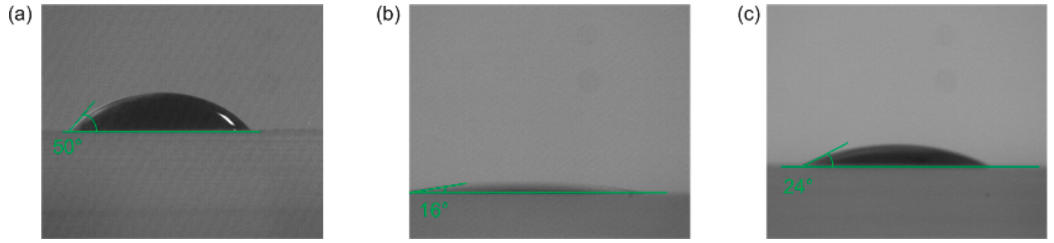

Figure 3. Contact angle measurement for droplets of PEDOT:PSS in aqueous solution on CNTs before (a) and after plasma (b). (c) Contact angle of a droplet of PEDOT:PSS diluted in IPA with a ratio of 1:3.

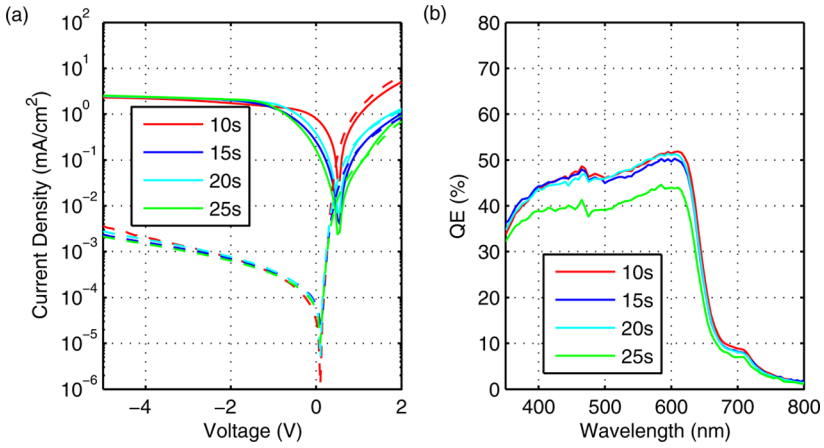

Figure 4. (a) Dark (dashed lines) and illuminated (solid lines) *JV* characteristics of OPDs obtained spray-coating PEDOT:PSS in aqueous solution and P3HT:PCBM blend on structured plasma-treated CNTs, increasing spraying time of the PEDOT:PSS layer. (b) EQE of the same samples.

enhancement in wettability corresponded to a 12 s exposition in a microwave low-pressure plasma asher (100 W, 0.3 mbar)

Optical microscope observations (Supporting Information, Figure S3) and contact angle measurements (Figure 3) show how a very mild microwave oxygen plasma treatment in a faradaic cage is effective in making the CNT network surface more hydrophilic. The most evident consequence of the plasma treatment is a strong reduction in the contact angle to 16° and a better merging, evident from the optical microscope. The droplets merge together leading to a uniform and continuous film.

The reduced contact angle and better spreading of the droplets, however, do not lead to any improvement in the characteristics of the diodes. If compared to the photodiodes fabricated on untreated CNT electrodes, the EQE range is even reduced, being on average below 50%, as shown in Figure 4. Moreover, the linear characteristics of the photodiodes show a strong "s-shape" (Supporting Information, Figure S2) in proximity of the zero crossing, s fact that is usually attributed to traps and defect-induced charge accumulations.[31] The only benefit is an increase in yield to 60% caused by enhanced wetting and hence improved planarization.

Sheet resistance measurements of the CNT film before and after plasma treatment demonstrated how the resistance of the films increased 30%, whereas the transmittance of the film stayed constant. Nevertheless, this increase in resistance is not enough to justify such a decrease in EQE and the modification in the shape of the characteristics.

For a better understanding of this phenomenon, the CNT film was investigated with Raman spectroscopy before and after mild O_2 plasma treatment. The ratio of the peak in the G band over the peak in the D band of the Raman spectrum is a figure of merit for the CNT film (the higher the ratio, the more defect free the film). Figure 5 shows the Raman spectra of the

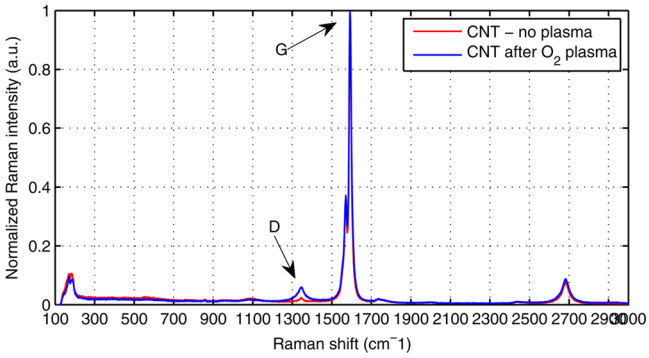

Figure 5. Raman spectra of a CNT film before (red) and after plasma (blue).

untreated and treated CNT films, from which the G/D ratios are extrapolated for the plasma-treated and untreated layers with values of 16.83 and 50, respectively.

Formation of defect centers worsens the electrical interface between CNTs and PEDOT:PSS, hence leading to the reported substantial degradation of the performances of the devices. Consequently, even if the yield is increased at around 60%, the plasma treatment cannot be considered an appropriate solution.

However, as reported in the literature,[13,33] mixing a solvent with a high boiling point and low vapor pressure (primary solvent) with a solvent with a lower boiling point and a higher vapor pressure (secondary solvent) can bring better deposition results. In fact, the secondary solvent reduces the surface tension and evaporates faster, enhancing the merging of the droplets while leading to a better uniformity and substrate coverage by means of Marangoni flows.

Since PEDOT:PSS is purchased in aqueous solution a good miscibility with 2-isopropyl alcohol (IPA) is obtained. The ratio of 1:3 (1 part of PEDOT:PSS in 3 parts of IPA) was found to be optimal for ultrasonic spray deposition on ITO substrates.[13] Morover, IPA is characterized by a boiling point of 82.6 °C and a vapor pressure of 13.33 kPa at 40 °C (versus 100 °C and 7.4 kPa for water, respectively) representing a good choice for a secondary solvent. The contact angle was reduced from 50° to 24°, as shown in Figure 3; optical microscope (Figure S3, Supporting Information) and profilometer inspections confirm the desired enhancement.

Figure 6 shows the $J-V$ characteristics and EQE of photodiodes fabricated with this formulation which present dark current densities on the order of magnitude of 10^{-3} mA/cm^2 at −5 V, average rectification ratios of 4 orders of magnitude, and EQE up to 65%. The optimum thickness of the PEDOT:PSS layer was found to be around 50 nm and could be finely and reliably regulated simply through regulation of the spraying time.

The optimization process developed so far was concentrated on the amelioration of the performances of the diodes. However, if compared to reference photodiodes with ITO electrodes (Supporting Information, Figure S1), high dark current is encountered, and even if an accurate processing of the samples is kept, only up to 60% of the devices were properly functioning. Since the average roughness of the CNT layer is not enough to justify an excessive amount of shunt paths in the devices,[25] the rise in dark current can be related to the bundles of nanotubes "spiking" in the bulk heterojunction. The presence of these strong irregularities creates local paths with a lower shunt resistance and low photoreactivity, resulting in a higher dark current and a locally lower photocurrent. Moreover, if these bundles are long and numerous enough to form a complete conductive path from cathode to anode electrodes, the fabrication process is not reliable and the devices are short circuited. These issues are well known in the literature and typical for devices based on random network of nanowires, as reported, for instance, by Lee et al.[34] and Leem et al.[35] In particular, one possible solution was reported in the latter work, consisting in fabricating devices with thick PEDOT:PSS layers. Although this approach solves the yield-related issues, it reduces even further the EQE and the photocurrent while it rises the dark current. Another approach, which is the one we pursued, is increasing the thickness of the bulk heterojunction. Since a high reverse bias can be applied to the diode, the electric field in the BHJ can still be high enough to guarantee charge separation and transport of carriers to the electrodes.

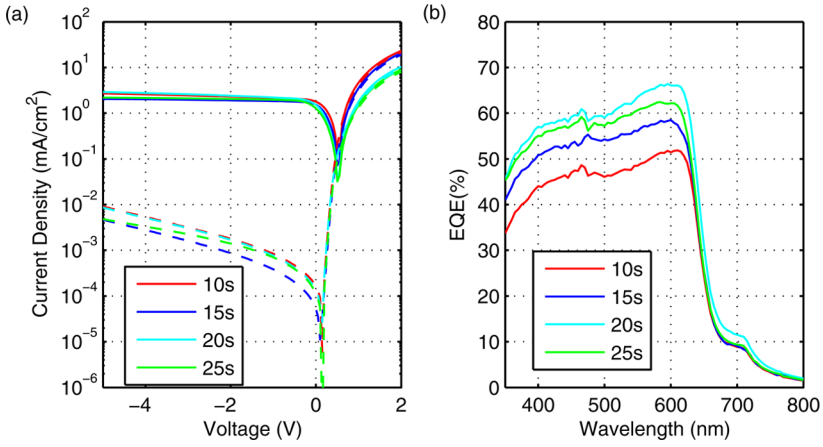

Figure 6. (a) Dark (dashed lines) and illuminated (solid lines) *JV* characteristics of OPDs obtained spray-coating PEDOT:PSS diluted in IPA and P3HT:PCBM blend on structured CNTs, increasing spraying time of the PEDOT:PSS layer. (b) EQE of the same samples.

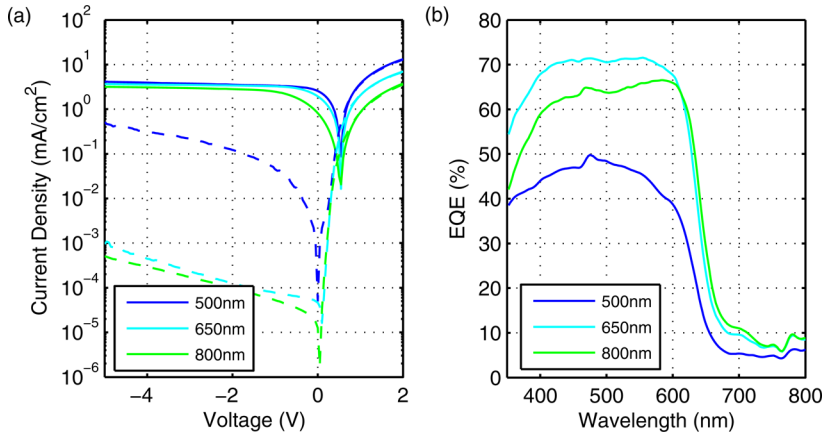

Figure 7. (a) Dark (dashed lines) and illuminated (solid lines) *JV* characteristics of OPDs for different thickness (500, 650, 800 nm) of the active layer. (b) EQE of the same samples.

We hence investigated how the dark current and the presence of "hot spots" changed with an increase in the thickness of the blend with means of two different analysis methods: Measurement of the $J-V$ characteristics in dark condition and under illumination and measurement of a spatially resolved EQE, keeping the sample in dark condition and moving a focused light spot on the active area of the sample recording the photocurrent generated as a reaction to the illumination of the device in that spot.

Figure 7 shows a comparison between the $J-V$ characteristics of devices with different active-layer thickness. A thickness of the active layer below 600 nm resulted in very high dark currents (above 10^{-2} mA/cm^2 at −5 V) and low on−off and rectification ratios (less than 2 orders of magnitude). The best devices could be fabricated with BHJ thickness of 650 and 800 nm, and the dark currents lowered down to 4×10^{-4} mA/cm^2 in the case of the thicker devices.

While the decrease in dark current gives a direction to follow to obtain better photodiodes, nothing can be stated on the spatial uniformity of the light responsivity. The presence of areas in which the photocurrent is not uniform could be, however, associated with shunt paths, as previously described. One possible method to investigate this phenomenon is by illuminating a defined area of the photodiode with monochromatic light and recording the output current, hence obtaining a spatially resolved EQE. A smaller light spot results in a higher resolution, thereby enhancing the ability to detect irregularities in light conversion. Measuring the spatially resolved EQE of photodiodes fabricated with different BHJ thicknesses can thus provide a better understanding of the relation between this parameter and the presence of shunt paths.

In order to measure the spatially resolved EQE, a focused light spot (λ = 550 nm, spot area (30 × 30) μm^2) was directed toward the sample through an inverted microscope. The sample was then moved with steps of 30 μm in the x and y directions to cover the whole area. Figure 8a shows how the thinnest device (500 nm active layer thickness) presented strong nonhomogeneities and extensive areas in which the response to light was very modest. Increasing the thickness of the BHJ to 650 nm (Figure 8b) leads to a higher uniformity and to significant reduction of "hot" and "cold" spots. This goes together with a substantial increase in the EQE that is above 70% for the working devices with a fabrication yield of 75%. Finally, the thickest BHJ layer brought to a totally uniform EQE on the entire area of the considered sample (Figure 8c) to a yield above 90% and still to a high overall EQE (above 65%) and dark currents as low as 10^{-4} mA/cm^2.

Table 1 shows the yield for the different combination of thickness and fabrication methods presented in this work.

Once the whole process has been optimized on glass, with minor adjustments in process parameters (in particular the annealing times were reduced in order to avoid any mechanical integrity impairment) it could be replicated on a flexible substrate using a polyethylene terephthalate (PET) thin foil.

The structure consisted of two stripes of CNTs with a sheet resistance of 200 Ω/sq, 50 nm PEDOT:PSS, 800 nm P3HT:PCBM, 1 nm of LiF, and 120 nm of aluminum, just as the best ones on glass.

Measurements of $J-V$ characteristics and EQE (Figure 9) show how the flexible devices exhibit a performance comparable to the ones on glass. We achieve on−off ratios of 4 orders of magnitude, dark current densities lower than 5×10^{-4} mA/cm^2, and EQE as high as 65%. The inset in Figure 9b shows the mechanical flexibility of the photodiodes obtained with the described deposition steps. Demonstrating the feasibility of fully sprayed devices on plastic substrates paves the way for the simple and cost-effective realization of conformable devices such as flexible scanners or curved photodetectors to be used in biomedical applications. Although similar devices are already reported in the literature,[36] they can currently only be fabricated through small molecule evaporation and use of expensive and brittle TCOs. It must be additionally noted that unlike optoelectronic devices fabricated by spray pyrolysis,[23] our entire fabrication process utilizes temperatures below 125 °C. This factor, along with the choice of avoiding any acid treatments, implied a straightforward adaptation of the deposition process from glass to plastic substrates. This once more proves spray deposition to be a versatile and easily adaptable technique for plastic electronics.

After demonstration of a feasible process for production of flexible photodiodes, further fine optimization of the performances of the device can be conducted. It is in fact interesting to notice that the EQE of a photodiode is influenced by several factors, and among them, it is important to highlight the dependence on transmittance, serial, and shunt resistance. If, on the one hand, the shunt resistance is fixed by the structure and the materials used for the bulk heterojunction, on the other hand, both the transmittance and the serial resistance are related to the physical characteristics of the electrodes.

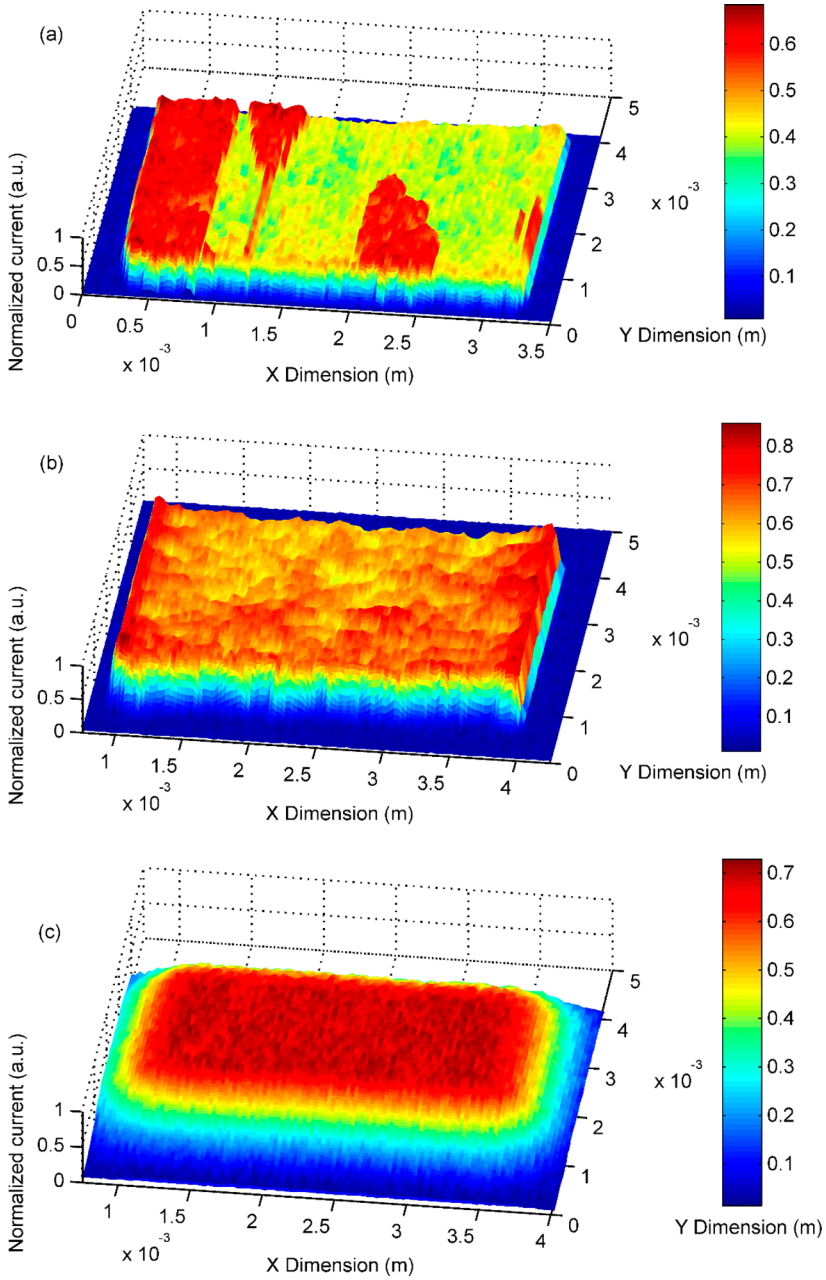

Figure 8. Spatially resolved EQE on the active area for different blend thickness: (a) 500, (b) 650, and (c) 800 nm.

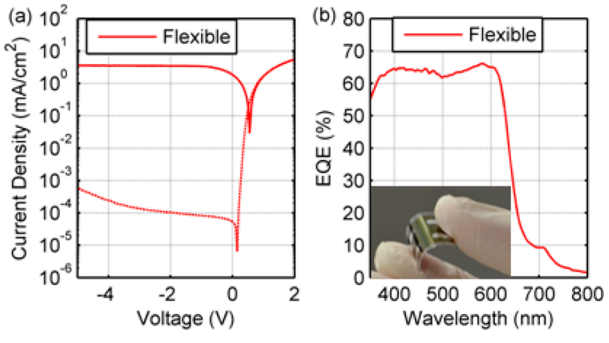

Figure 9. (a) Dark (dashed lines) and illuminated (solid lines) *JV* characteristics of OPDs obtained spray-coating PEDOT:PSS diluted in IPA and blend on PET substrate. (b) EQE of the same samples. (Inset) Fabricated flexible diode.

As we previously stated, the Tinkham formula relates the transmittance of the thin film to its sheet resistance, and this can be easily modulated with the thickness of the conducting layer.[25] This flexibility gives one more degree of freedom that has to be taken in account and carefully set. In fact, high sheet resistance means high serial resistance and, hence, electric losses. On the other side, low sheet resistance corresponds to lower transmittance, meaning that less photons can reach the bulk of the photodiode. This effect can be examined by means of the simple diode circuital model (schematic depicted in Figure S5, Supporting Information) in the overall EQE, which is the ratio of the extracted electrons to the incident photons successfully transferred to the load

$$\mathrm{EQE}(\lambda) = \eta_0(\lambda)^* T_{\mathrm{CNT}}(\lambda)^* \frac{R_\mathrm{p}}{R_\mathrm{p} + R_\mathrm{s}}$$

where η_0 is the internal quantum efficiency that the device would have if the anode would have been completely transparent and the diode presented serial resistance negligible with respect to the shunt resistance (this value is close to 90% for optimized BHJ with P3HT and PCBM, as reported, for instance, by Schilinsky et al.[37]). T_{CNT} is the transmittance of the CNT film; R_p, and R_s are shunt and serial resistance, respectively.

At this point, taking in account that R_s can be considered proportional to the sheet resistance and substituting the transmittance with the Tinkham formula 1 it can be rewritten as

$$EQE = \eta_0 * \frac{\gamma^2 R_{sheet}^2}{(\alpha R_{sheet} + 1)(\gamma R_{sheet} + 60\pi)^2}$$

Further details of the derivation are presented in the Supporting Information. Here, γ is the experimentally evaluated ratio between optical and dc conductivities, shown in the Experimental Methods. The factor $\alpha = R_s/(R_p R_{sheet})$ was estimated experimentally on several devices (shunt and serial resistances were evaluated with a first-order approximation, and the parameter was calculated) and gave a result of $\alpha = (950 \pm 20) \times 10{-}6\ \Omega^{-1}$. η_0 was considered to be equal to 0.9, as previously discussed.

Figure 10 shows the measured values of EQE for a given couple (T, R_{sheet}) of the transparent thin film and the fit with the theoretical curve extrapolated by the circuital model and the physical assumptions. The good fitting of the theoretical curve to the experimental values gives the formula a "predictive value" to find the optimum. Using this approach, a favorable choice of the transparent electrode thickness can be performed even if it could seem for some reasons counterintuitive, for instance, because the chosen R_{sheet} value could be considered relatively high, and gives in fact the best results.

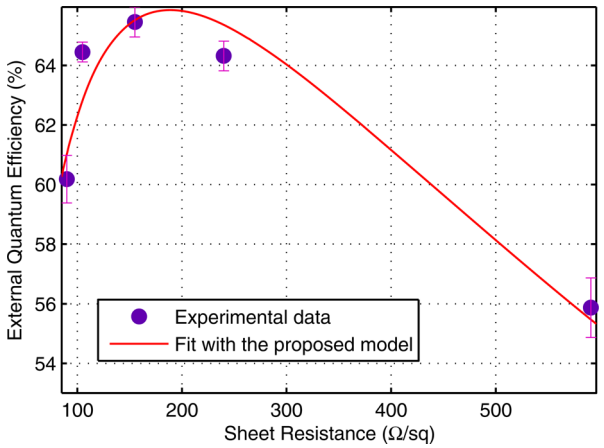

Figure 10. Experimental data (circles) and plot of the formula (solid line) of the EQE as a function of sheet resistance. $R^2 = 0.92$.

CONCLUSIONS

A process for state-of-the-art performance, TCO-free, carbon-based, and fully sprayed organic photodiodes has been proposed and optimized. Only the cathode was obtained through physical vapor deposition.

First, we analyzed and solved specific issues of the process related to the interfaces and the poor wettability of the CNT film. The two-solvent system proved to be the most suitable choice since it lead to higher yields and better performances. Moreover, the good wetting capabilities of the solution rendered it useful to reduce the PEDOT:PSS film thickness, being particularly interesting to enhance the characteristics of both sprayed OPDs on ITO and on CNTs. In order to reduce formation of hot spots, a BHJ thickness sufficient to guarantee low dark currents and high yields was chosen. Devices exhibited dark currents as low as 10^{-4} mA/cm^2, on–off ratios of 4 orders of magnitude, EQE up to 65%, and fabrication yields above 90%. The acquired expertise was then used to fabricate a flexible photodiode with performance identical to the ones with CNT electrodes on glass and comparable in terms of on–off ratios and EQEs to the reference on glass. Finally, fine tuning of the device was performed using a model developed to find the optimum compromise between transmittance and sheet resistance of the transparent electrode, taking into account the correlation of the two parameters given by the Tinkham formula.

ASSOCIATED CONTENT

Supporting Information

Reference characteristics for spray-coated photodiodes with ITO electrodes, linear characteristics at the zero crossing, optical microscope images, and details on the calculations for the EQE formula. This material is available free of charge via the Internet at http://pubs.acs.org.

AUTHOR INFORMATION

Corresponding Author

*E-mail: Aniello.falco@nano.ei.tum.de.

Author Contributions

The manuscript was written through contributions of all authors. All authors have given approval to the final version of the manuscript.

Notes

The authors declare no competing financial interest.

ACKNOWLEDGMENTS

This work is partially supported by the DFG within the German Excellence Initiative through the cluster of excellence "Nanosystems Initiative Munich" (NIM), the Free State of Bavaria through the research network "Solar Technologies Go Hybrid" (SolTech), the European Union through FP7-PEOPLE-2012-ITN 316832-OLIMPIA, the TUM Graduate School (TUM-GS), the Deutscher Akademischer Austauschdienst (DAAD) and the Conferenza dei Rettori delle Universitá Italiane (CRUI) through the Vigoni Program.

REFERENCES

(1) Gunes, S.; Neugebauer, H.; Sariciftci, N. S. Conjugated Polymer-Based Organic Solar Cells. *Chem. Rev.* **2007**, *107*, 1324–1338.
(2) Li, G.; Zhu, R.; Yang, Y. Polymer Solar Cells. *Nat. Photonics* **2012**, *6*, 153–161.
(3) Baeg, K.-J.; Binda, M.; Natali, D.; Caironi, M.; Noh, Y.-Y. Organic Light Detectors: Photodiodes and Phototransistors. *Adv. Mater. (Weinheim, Ger.)* **2013**, *25.31*, 4267–4295.
(4) Gruner, G. Carbon Nanotube Films for Transparent and Plastic Electronics. *J. Mater. Chem.* **2006**, *16*, 3533–3539.
(5) Cao, Q.; Rogers, J. A. Ultrathin Films of Single-Walled Carbon Nanotubes for Electronics and Sensors: A Review of Fundamental and Applied Aspects. *Adv. Mater. (Weinheim, Ger.)* **2009**, *21*, 29–53.

(6) Hu, L.; Hecht, D. S.; Grüner, G. Carbon Nanotube Thin Films: Fabrication, Properties, and Applications. *Chem. Rev.* **2010**, *110*, 5790−5844.
(7) Zhang, D.; Ryu, K.; Liu, X.; Polikarpov, E.; Ly, J.; Tompson, M. E.; Zhou, C. Transparent, Conductive, and Flexible Carbon Nanotube Films and Their Application in Organic Light-Emitting Diodes. *Nano Lett.* **2006**, *6*, 1880−1886.
(8) Chien, Y.-M.; Lefevre, F.; Shih, I.; Izquierdo, R. A Solution Processed Top Emission OLED with Transparent Carbon Nanotube Electrodes. *Nanotechnology* **2010**, *21*, 134020.
(9) Tenent, R. C.; Barnes, T. M.; Bergeson, J. D.; Ferguson, A. J.; To, B.; Gedvilas, L. M.; Heben, M. J.; Blackburn, J. L. Ultrasmooth, Large-Area, High-Uniformity, Conductive Transparent Single-Walled-Carbon-Nanotube Films for Photovoltaics Produced by Ultrasonic Spraying. *Adv. Mater. (Weinheim, Ger.)* **2009**, *21*, 3210−3216.
(10) Trottier, C. M.; Glatkowski, P.; Wallis, P.; Luo, J. Properties and Characterization of Carbon-Nanotube-Based Transparent Conductive Coating. *J. Soc. Inf. Disp.* **2005**, *13*, 759.
(11) Cho, D.-Y.; Eun, K.; Choa, S.-H.; Kim, H.-K. Highly Flexible and Stretchable Carbon Nanotube Network Electrodes Prepared by Simple Brush Painting for Cost-Effective Flexible Organic Solar Cells. *Carbon* **2014**, *66*, 530−538.
(12) Tedde, S. F.; Kern, J.; Sterzl, T.; Fürst, J.; Lugli, P.; Hayden, O. Fully Spray Coated Organic Photodiodes. *Nano Lett.* **2009**, *9*, 980−983.
(13) Girotto, C.; Moia, D.; Rand, B. P.; Heremans, P. High-Performance Organic Solar Cells with Spray-Coated Hole-Transport and Active Layers. *Adv. Funct. Mater.* **2011**, *21*, 64−72.
(14) Kim, S.; Yim, J.; Wang, X.; Bradley, D. D. C.; Lee, S.; DeMello, J. C. Spin- and Spray-Deposited Single-Walled Carbon-Nanotube Electrodes for Organic Solar Cells. *Adv. Funct. Mater.* **2010**, *20*, 2310−2316.
(15) Abdellah, A.; Baierl, D.; Fabel, B.; Lugli, P.; Scarpa, G. Exploring Spray Technology for the Fabrication of Organic Devices Based on Poly(3-hexylthiophene). *IEEE Int. Conf. Nanotechnol., 9th* **2009**, 831−934.
(16) Abdellah, A.; Fabel, B.; Lugli, P.; Scarpa, G. Spray Deposition of Organic Semiconducting Thin-films: Towards the Fabrication of Arbitrary Shaped Organic Electronic Devices. *Org. Electron.* **2010**, *11*, 1031−1038.
(17) Abdellah, A.; Virdi, K. S.; Meier, R.; Döblinger, M.; Müller-Buschbaum, P.; Scheu, C.; Lugli, P.; Scarpa, G. Successive Spray Deposition of P3HT/PCBM Organic Photoactive Layers: Material Composition and Device Characteristics. *Adv. Funct. Mater.* **2012**, *22*, 4078−4086.
(18) Vak, D.; Kim, S.-S.; Jo, J.; Oh, S.-H.; Na, S.-I.; Kim, J.; Kim, D.-Y. Fabrication of Organic Bulk Heterojunction Solar Cells by a Spray Deposition Method for Low-cost Power Generation. *Appl. Phys. Lett.* **2007**, *91*, 081102−1−081102−3.
(19) Steirer, K. X.; Reese, M. O.; Rupert, B. L.; Kopidakis, N.; Olson, D. C.; Collins, R. T.; Ginley, D. S. Ultrasonic Spray Deposition for Production of Organic Solar Cells. *Sol. Energy Mater. Sol. Cells* **2009**, *93*, 447−453.
(20) Barnes, T. M.; Bergeson, J. D.; Tenent, R. C.; Larsen, B. a.; Teeter, G.; Jones, K. M.; Blackburn, J. L.; Van de Lagemaat, J. Carbon Nanotube Network Electrodes Enabling Efficient Organic Solar Cells without a Hole Transport Layer. *Appl. Phys. Lett.* **2010**, *96*, 243309.
(21) Binda, M.; Natali, D.; Iacchetti, A.; Sampietro, M. Integration of an Organic Photodetector onto a Plastic Optical Fiber by Means of Spray Coating Technique. *Adv. Mater. (Weinheim, Ger.)* **2013**, *25*, 4335−4339.
(22) Na, S.-I.; Yu, B.-K.; Kim, S.-S.; Vak, D.; Kim, T.-S.; Yeo, J.-S.; Kim, D.-Y. Fully Spray-Coated ITO-Free Organic Solar Cells for Low-cost Power Generation. *Sol. Energy Mater. Sol. Cells* **2010**, *94*, 1333−1337.
(23) La Notte, L.; Mineo, D.; Polino, G.; Susanna, G.; Brunetti, F.; Brown, T. M.; Di Carlo, A.; Reale, A. Fabrication of Fully-Spray-Processed Organic Photovoltaic Modules by using an Automated Process in Air. *Energy Technol. (Weinheim, Ger.)* **2013**, *1*, 757−762.
(24) Strano, M. S.; Moore, V. C.; Miller, M. K.; Allen, M. J.; Haroz, E. H.; Carter, K.; R. H, H.; Smalley, R. E. The Role of Surfactant Adsorption during Ultrasonication in the Dispersion of Single-Walled Carbon Nanotubes. *J. Nanosci. Nanotechnol.* **2003**, *3*, 81−86.
(25) Abdelhalim, A.; Abdellah, A.; Scarpa, G.; Lugli, P. Fabrication of Carbon Nanotube Thin films on Flexible Substrates by Spray Deposition and Transfer Printing. *Carbon* **2013**, *61*, 72−79.
(26) Tinkham, M. Energy Gap Interpretation of Experiments on Infrared Transmission through Superconducting Films. *Phys. Rev.* **1956**, *104*, 845.
(27) Parekh, B. B.; Fanchini, G.; Eda, G.; Chhowalla, M. Improved Conductivity of Transparent Single-Wall Carbon Nanotube Thin Films via Stable Postdeposition Functionalization. *Appl. Phys. Lett.* **2007**, *90*, 121913.
(28) Han, K. N.; Li, C. A.; Ngoc Bui, M.-P.; Seong, G. H. Patterning of Single-Walled Carbon Nanotube Films on Flexible, Transparent Plastic Substrates. *Langmuir* **2010**, *26*, 598−602.
(29) Leem, D.-S.; Kim, S.; Kim, J. W.; Sohn, J. I.; Edwards, A.; Huang, J.; Wang, X.; Kim, J.-J.; Bradley, D. D. C.; Demello, J. C. Rapid Patterning of Single-wall Carbon Nanotubes by Interlayer Lithography. *Small* **2010**, *6*, 2530−2534.
(30) Chirila, V.; Marginean, G.; Brandl, W. Effect of the Oxygen Plasma Treatment Parameters on the Carbon Nanotubes Surface Properties. *Surf. Coat. Technol.* **2005**, *200*, 548−551.
(31) Baierl, D.; Fabel, B.; Gabos, P.; Pancheri, L.; Lugli, P.; Scarpa, G. Solution-Processable Inverted Organic Photodetectors Using Oxygen Plasma Treatment. *Org. Electron.* **2010**, *11*, 1199−1206.
(32) Petrosino, M.; Vacca, P. The Effect of ITO Surface Energy on OLED Electrical Properties. *IWPSD,14th* **2007**, 1−4.
(33) Azzellino, G.; Grimoldi, a; Binda, M.; Caironi, M.; Natali, D.; Sampietro, M. Fully Inkjet-Printed Organic Photodetectors with High Quantum Yield. *Adv. Mater. (Weinheim, Ger.)* **2013**, *25*, 6829−6833.
(34) Lee, J.-Y.; Connor, S. T.; Cui, Y.; Peumans, P. Solution-Processed Metal Nanowire Mesh Transparent Electrodes. *Nano Lett.* **2008**, *8*, 689−692.
(35) Leem, D.-S.; Edwards, A.; Faist, M.; Nelson, J.; Bradley, D. D. C.; De Mello, J. C. Efficient Organic Solar Cells with Solution-Processed Silver Nanowire Electrodes. *Adv. Mater. (Weinheim, Ger.)* **2011**, *23*, 4371−4375.
(36) Someya, T.; Kato, Y.; Iba, S.; Noguchi, Y.; Sekitani, T.; Kawaguchi, H.; Sakurai, T. Integration of Organic FETs With Organic Photodiodes for a Large Area, Flexible, and Lightweight Sheet Image Scanners. *IEEE Trans. Electron Devices* **2005**, *52*, 2502−2511.
(37) Schilinsky, P.; Waldauf, C.; Brabec, C. J. Recombination and Loss Analysis in Polythiophene Based Bulk Heterojunction Photodetectors. *Appl. Phys. Lett.* **2002**, *81*, 3885.